



Reimagining the Water Snowline

Arthur D. Bosman and Edwin A. Bergin

Department of Astronomy, University of Michigan, 323 West Hall, 1085 S. University Avenue, Ann Arbor, MI 48109, USA; arbos@umich.edu*Received 2021 May 28; revised 2021 August 11; accepted 2021 August 15; published 2021 August 26*

Abstract

Water is a molecule that is tightly related to many facets of star and planet formation. Water's abundance and distribution, especially the location of its snowline has thus been the subject of much study. While water is seen to be abundant in the inner region of protoplanetary disks in infrared spectroscopy, detections of water in the disk in the submillimeter are rare, with only one detection toward AS 205. Here we put the multitude of nondetections and the single detection into context of recent physicochemical models. We find that the 321.2257 GHz ($10_{2,9}-9_{3,6}$) line detection toward AS 205 is inconsistent with a normal inner disk temperature structure and that the observed line must be masing. Furthermore, the emitting area derived from the line width, together with published analyses on water in disks around T-Tauri stars implies that the water snowline in the disk surface is at the same location as the snowline in the midplane. We propose that this is caused by vertical mixing continuously sequestering water from the warm surface layers into the cold disk midplane.

Unified Astronomy Thesaurus concepts: [Protoplanetary disks \(1300\)](#); [Astrochemistry \(75\)](#); [Chemical abundances \(224\)](#); [Submillimeter astronomy \(1647\)](#)

1. Introduction

The existence of water on a terrestrial planet is one of the main requirements of life and the Earth's oceans have an enormous impact on life's origin and evolution (Cockell et al. 2016; Lingam & Loeb 2019). The trail of water and its origin is thus one that has had strong astrophysical focus (see, e.g., van Dishoeck et al. 2021 for an extensive review) and this clearly extends to searching for water in the exoplanet atmospheres (e.g., Madhusudhan 2019).

Our current understanding suggests that the Earth formed situated within the radius of the water snowline, the transition between vapor and ice phases of water (e.g., Hayashi 1981). As such very little water was present on solids during Earth's assembly. Water must have been supplied from greater distances, beyond the water snowline where icy bodies, whether planetesimals or pebbles, are found in abundance (Morbidelli et al. 2000; Ida et al. 2019). In the solar system, the water snowline location seems to have been around 2.7 au, in the middle of the asteroid belt. However, the influence of the solar system gas giants, Jupiter and Saturn, could have modified this record (Morbidelli et al. 2016; Kruijer et al. 2020). The water snowline in the early solar system is predicted to be far closer to the Sun than 2.7 au, with values closing into 1 au, the Earth's orbit (e.g., Mulders et al. 2015).

The location of the snowline is dependent on the stellar radiation field, as well as the amount of viscous heating (e.g., Harsono et al. 2015). The location of the water snowline is therefore expected to evolve and its location directly informs on the potential supply terms of water for habitable worlds (Ida et al. 2019).

Water from within the water snowline has been observed with infrared spectroscopy (e.g., Carr & Najita 2008; Pontoppidan et al. 2014). Spitzer-IRS observations show that water is abundant in the inner region of protoplanetary disks, with an emitting region that has a 1–3 au radius based on the LTE line modeling (Pontoppidan et al. 2010b; Carr & Najita 2011; Salyk et al. 2011b). This is confirmed by velocity resolved mid-infrared spectroscopy (Pontoppidan et al. 2010a; Najita et al. 2018;

Salyk et al. 2019). The H_2O lines in the mid-infrared have high upper level energies, >3000 K for the velocity resolved lines and thus only trace hot gas. It is not directly clear if the extent of the emitting area is set by the abundance structure of H_2O or the temperature in the inner disk. As such these emitting area's cannot be directly used to infer the H_2O snowline. This is further complicated by the fact that these lines only trace the upper atmosphere as the midplane is obscured by optically thick dust. Any snowline inferred would thus be the surface snowline.

Blevins et al. (2016) have attempted to break this degeneracy for four well studied disks, using lower upper level energy water lines observed by Hershell between 75 and 180 μm to probe the colder ($T > 300$ K) regions of the disk surface. They find that the H_2O abundance does strongly drop, even in the surface layers of the disk where H_2O should not freeze-out. The radius at which the H_2O abundance drops, is inferred to be larger than emitting radii inferred from the infrared lines by a factor of ~ 2 for three out of the four sources.¹ Implying that both excitation and abundance are important in setting infrared H_2O line strength.

Submillimeter observations with ALMA are in theory perfect to supplement the existing observations. The orders of magnitude lower dust opacity at submillimeter wavelengths as well as the availability of H_2^{18}O lines allow the observations to probe deep into the disk and the low upper level energies (<500 K) are more sensitive to gas around the midplane water snowline (e.g., Notsu et al. 2018). The search for water with ALMA has so far mostly led to upper limits, even in warmer and younger disks (Notsu et al. 2019; Harsono et al. 2020, and Section 4).

Only one detection of water from the inner disk reservoir has been made with ALMA toward solar analog AS 205 ($0.87 M_{\odot}$; Carr et al. 2018). They report a detection of the 321.2257 GHz o- H_2O ($10_{2,9}-9_{3,6}$) water line. This line has an upper level energy of 1861 K and an Einstein A coefficient of 5.048×10^{-6} . Interestingly the lower energy 322.4652 GHz

¹ The fourth sources, RNO 90, has an inferred abundant H_2O radius $\sim 8\times$ the area necessary for the IR lines.

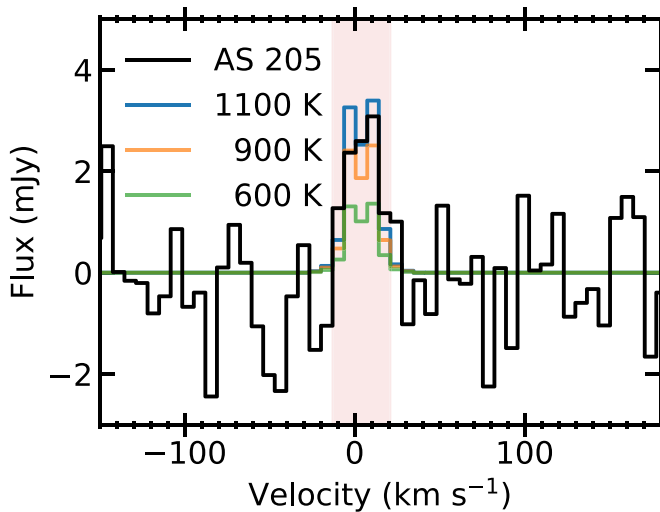


Figure 1. The $10_{2,9}\text{--}9_{3,6}$ water line observed toward AS 205 compared to power-law intensity models with an extent of 1.8 au. Labels denote the temperature assumed at 1.8 au, and the temperature behaves as $T(R) = T_{1.8\text{ au}}(R/1.8)^{-0.5}$. Very high temperatures at 1.8 au are necessary to produce the observed line.

$p\text{-H}_2^{18}\text{O}$ ($5_{1,5}\text{--}4_{2,2}$) line, with an upper level energy of 468 K and Einstein A coefficient of 1.045×10^{-5} , was not detected. In this Letter we will interpret the ALMA water detection and nondetections and discuss the implications for the structure of the water reservoir around the water snowline.

2. Water Emission from within the Midplane Snowline

We re-reduced the AS 205 data from project 2016.1.00549.S (PI: Carr, J.) using CASA version 5.6.1. After the standard pipeline calibrations² we performed two rounds of phase only self-calibration and one round of amplitude self-calibrations, giving a signal-to-noise ratio increase on the continuum of a factor of 14. The lines were then imaged using Briggs weighting with a robust value of 0.5, binning to a 6.8 km s^{-1} channel width following (Carr et al. 2018). We do not perform any clean iterations. The spectrum for the 321.226 GHz line extracted on the peak position of the continuum is shown in Figure 1. The integrated line flux between -14 and 22 km s^{-1} is $71 \pm 17\text{ mJy km s}^{-1}$, consistent with the values from Carr et al. (2018). We ran a couple of tests on the imaging and measure similar line fluxes from the product data, when imaging the measurement set before self-calibration, when using a different channel binning (5 km s^{-1} binning or a 3.4 km s^{-1} velocity shift) as well as when imaging with natural weighting. This implies that this is not a feature introduced by any of the steps in data reduction.

The line width, $\sim 20\text{ km s}^{-1}$, implies a small water emitting area especially considering the near face-on (20°) inclination of AS 205. Carr et al. (2018) find the emitting area to be constrained within a 1.8 au radius from of the line kinematics. This agrees with the emitting area extracted from line kinematics and LTE modeling of mid-infrared lines origination from the AS 205 disk (Salyk et al. 2011b; Najita et al. 2018). We use this emitting area to extract the emission temperature of the water line. We assume a power-law temperature profile between 0.1 and 1.8 au with a power-law coefficient $q = -0.5$. For simplicity we will assume that the line is optically thick and

that the line width is given by the kinetic temperature at 1.8 au. The temperature at 1.8 au is varied to match the observed line strength.

Figure 1 shows the comparison between the observed water line and the power-law models. Very high temperatures ($>900\text{ K}$) at 1.8 au are necessary to reproduce the line flux. This temperature is significantly higher than previous temperatures derived from the inner 2 au for AS 205. Modeling of the Spitzer water lines implies a temperature of 450 K (Salyk et al. 2011b), which is consistent with the rotational temperature of the rovibrational ^{13}CO lines that have the same line width as the $10_{2,9}\text{--}9_{3,6}$ water line (Salyk et al. 2011a; Banzatti et al. 2017). Finally, Najita et al. (2018) find a temperature of 680 K to fit the velocity resolved $12.5\text{ }\mu\text{m}$ water lines also coming from within 2 au. The emission temperature necessary for the $10_{2,9}\text{--}9_{3,6}$ water line is thus anomalously high. Especially when considering that all the other observations trace high Einstein A coefficient lines with upper level energies $>3000\text{ K}$, significantly higher than the $10_{2,9}\text{--}9_{3,6}$ line upper level energy of $\sim 1800\text{ K}$. The other tracers should thus be tracing hotter gas.

The uncertainties in the observation allow for a larger emitting area, Carr et al. (2018) quote a 1σ range of 1.1–2.5 au. A larger emitting area would result in significantly lower emission temperatures required to reproduce the line. The $10_{2,9}\text{--}9_{3,6}$ line would still have to be optically thick, indicating a column of $>10^{19}\text{ cm}^{-2}$. At gas temperatures above 300 K, this gas would also contribute to the Spitzer spectra (e.g., Salyk et al. 2011b). If temperatures are below 300 K (i.e., much larger emitting area) the lower upper level energy H_2^{18}O lines have similar optical depths and should have been detected. They are not (see Section 4).

Assuming the same emitting region for the submillimeter and infrared lines, the high line strength of the $10_{2,9}\text{--}9_{3,6}$ line compared to the infrared lines can only be explained by assuming that this line is currently masing. The $10_{2,9}\text{--}9_{3,6}$ water line is often seen to be masing in star-forming regions where it traces high density shocks (e.g., Patel et al. 2007), as well as in the outflows of (post-)asymptotic giant branch stars (e.g., Gray et al. 2016). In these environments this line show masing behavior for H_2 densities below 10^{10} cm^{-3} (Neufeld & Melnick 1991; Gray et al. 2016).

It is very difficult to extract physical properties of the line emitting regions from maser lines, especially if there is only one (Neufeld & Melnick 1991). As such using this line for abundance determinations in the inner disk is going to be virtually impossible. However, the measured brightness does require a saturated maser, which puts a lower limit to the water column. For densities of 10^9 cm^{-3} the water maser saturates around a column of 10^{18} cm^{-2} (van der Tak et al. 2007; Daniel et al. 2011). Assuming a water abundance of 10^{-4} , this results in a H_2 column density of $\sim 10^{22}\text{ cm}^{-2}$. The density in the Bruderer et al. (2015) model reaches $\sim 5 \times 10^9\text{ cm}^{-3}$ at this column. This is on the high side for this line to be masing, but the density depends strongly of the assumed disk structure. Furthermore a water abundance elevated above 10^{-4} , for example, due to drift (e.g., Ciesla & Cuzzi 2006), would make it easier to get the required water column at a low enough density for maser activation.

The maser boost does make the line easier to detect. A thermal line with a 450 K emitting temperature and the same emitting region would not have been detected with 30 minutes of integration with ALMA. The maser boost allows us to use ALMA to probe the region inwards of the water snowline, and

² This was done with the pipeline of CASA version 4.7.2, for which the pipeline script was developed.

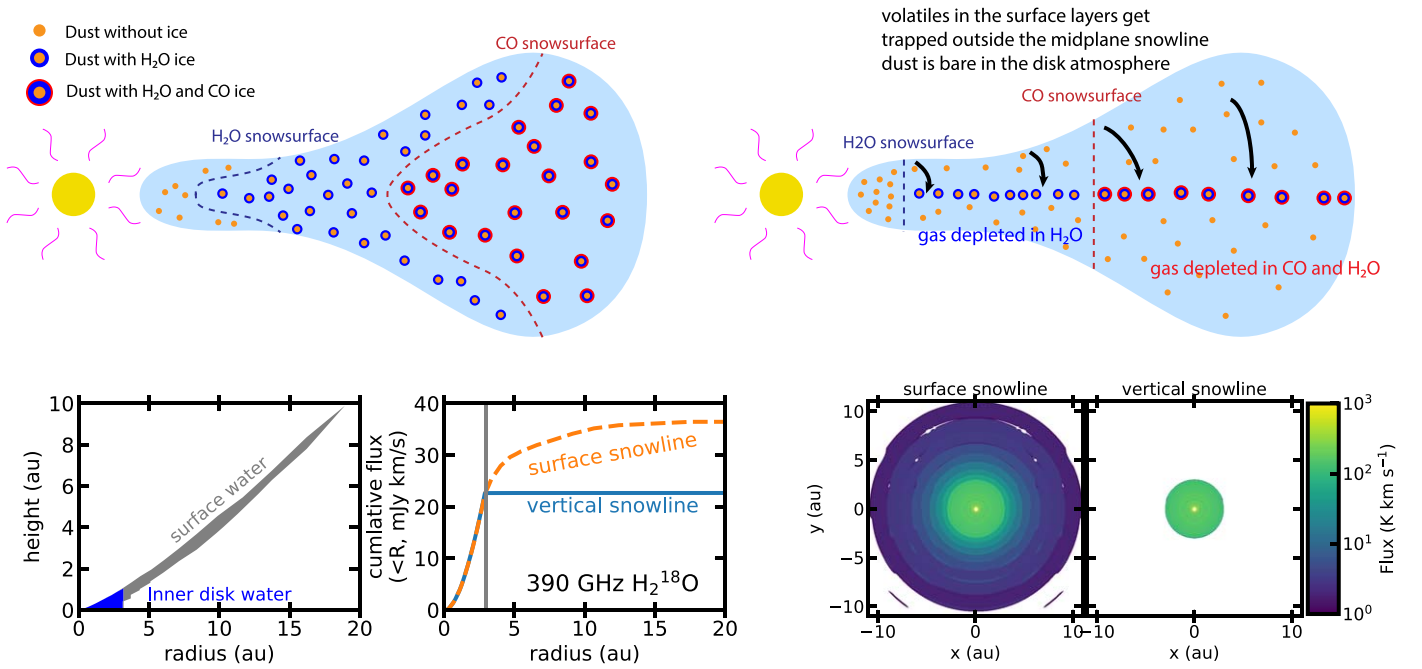


Figure 2. (Top) Schematic of the classical picture of the major H_2O and CO snow surfaces in a disk (left) and the behavior derived from observations (Blevins et al. 2016; Du et al. 2017; Zhang et al. 2019) and predicted by models (Krijt et al. 2016, 2020). (Bottom) Model predictions for water emission. Left panels show the gaseous water containing regions in a AS 205 disk model (Bruderer et al. 2015) with $T_{\text{dust}} > 150$ K and $A_V > 1$, split into the inner disk and surface reservoirs. The water abundance in the inner disk is assumed to be 10^{-4} while the surface layer water abundance is assumed to be 10^{-8} or 10^{-5} representing situations with a vertical and surface snowline. The rest of the panels show emission predictions for the $4_{1,4}-3_{2,1}$ H_2^{18}O line for these two models both as cumulative radial profiles as well as integrated line intensity.

using kinematical analysis allows us to determine the emitting region of the water lines observed in the infrared with Spitzer-IRS and JWST-MIRI providing an alternative to the challenging ground-based velocity resolved mid-infrared water observations (Najita et al. 2018; Salyk et al. 2019).

3. Reimagining the Water Snowline

The small water emitting area for the $10_{2,9}-9_{3,6}$ combined with a similar emitting area for many other water lines (Salyk et al. 2011b; Carr et al. 2018; Najita et al. 2018) implies that the water emitting area is strongly confined within the AS 205 disk. The nondetection of the H_2^{18}O lines further supports this and implies a small water emitting radius (Carr et al. 2018; Notsu et al. 2019, Section 4). In an AS 205 specific model, Bruderer et al. (2015) find that at ~ 2 au, the midplane temperature is around 200 K, the expected temperature of the H_2O snowline (assuming a density of 10^{16} cm^{-3} ; Harsono et al. 2015). For AS 205, the physical extent of the surface water reservoir thus seems to be as big as the midplane water reservoir. This is in conflict with the classical picture of the water snow surface (see Figure 2). This is inline with the observational results that consistently find a strong jump in the water abundance in the surface layers outside of the midplane snowline location (Meijerink et al. 2009; Bergin et al. 2010; Hogerheijde et al. 2011; Blevins et al. 2016).

This has previously been inferred as a drop of the water abundance due to inefficient H_2O formation in colder (< 300 K) gas (Blevins et al. 2016). However, not sequestering the elemental oxygen in water would imply a very high CO_2 abundance ($\sim 10^{-4}$ with respect to H_2), which is strongly in conflict with current observations (Pontoppidan & Blevins 2014; Bosman et al. 2017, 2018). Instead we propose that this drop in the water abundance is due to chemodynamical processing, analogous to

what happens in the outer disk with CO outside of the CO midplane snowline (Kama et al. 2016; Krijt et al. 2018, 2020).

In the outer disk CO is thought to be depleted by a combination of vertical mixing, dust settling and chemical processing. The vertical mixing moves gaseous CO from above the surface snowline to the midplane where it gets stuck on large settled grains, while chemical conversion transforms CO into less volatile species (CO_2 , H_2O , and CH_4), which also get stuck on the grains. This leads to a CO abundance that is 1–2 orders of magnitude lower in the disk surface. This is below the expected surface layer abundance even in gas and dust layers that are above the CO sublimation temperature. This can be clearly see in the CO abundance profiles from Zhang et al. (2019, Figure 8), which have an ISM CO abundance within the snowline, but a strongly depleted CO abundance outside, which implies the CO abundance lowers over the entire vertical extent of the disk. On a global scale, there thus is only a vertical snowline at the midplane snowline radius and no CO snow surface. This is shown schematically in Figure 2.

To explain the observed water abundance structures we invoke a similar effect near the H_2O snowline. Krijt et al. (2016) shows that in an isothermal column vertical mixing and dust growth can lead to strong water depletion above the water snow surface. This would naturally explain the strong jump in water abundance at the midplane snowline location.

This process would even help explain the relatively low CO_2 mid-infrared fluxes observed toward protoplanetary disks (Pontoppidan & Blevins 2014; Woitke et al. 2019). In the disk surface, CO_2 that is present will mostly be converted into H_2O and CO by the strong UV field and modest temperatures (100–300 K) in the disk surface between the H_2O and CO_2 icelines (e.g., Bosman et al. 2018). If the H_2O continuously gets sequestered into the midplane, this would remove the

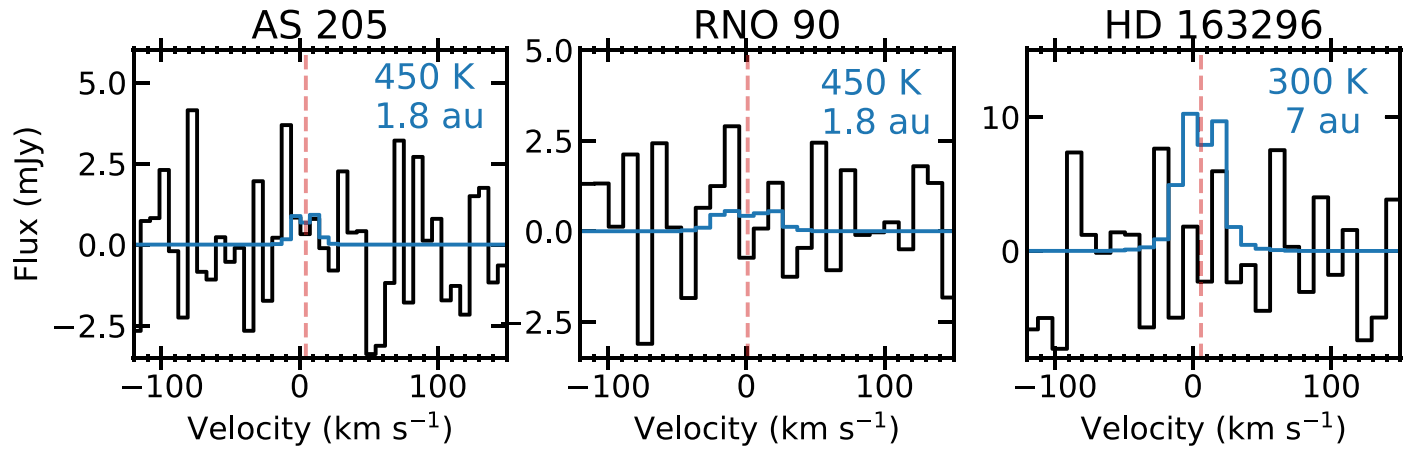


Figure 3. Nondetections of H_2^{18}O lines toward AS 205 N (322.465 GHz, $5_{1,5}-4_{2,2}$, left), and RNO 90 and HD 163296 (390.608 GHz, $4_{1,4}-3_{2,1}$, middle and right, respectively). Red vertical lines show the systemic velocity for the three systems. The blue line shows a power-law intensity model. For AS 205 and RNO 90 temperature and extent are chosen in rough correspondence to the temperatures and emitting areas derived from mid-infrared line modeling. In the case of HD 163296, the extent is given by the water snowline in the model from Notsu et al. (2016) with the temperature being the difference between the surface layer gas temperature and the midplane dust temperature at the midplane snowline location.

Table 1
Source Properties

Source	Stellar Mass (M_{\odot})	Stellar Luminosity (L_{\odot})	Distance (pc)	Inclination (deg)	Snowline Location (au)	References
AS 205	0.871	2	128	20	1.8	(1), (2)
RNO 90	1.5	4	125	37	1.5–11	(3), (4), (5)
HD 163296	2.0	17	101	46	7	(1), (6)

References. (1) Andrews et al. (2018), (2) Carr et al. (2018), (3) Salyk et al. (2011b), (4) Pontoppidan et al. (2011), (5) Blevins et al. (2016), and (6) Notsu et al. (2019).

oxygen necessary for CO_2 formation. This leaves the gas with only CO carrying a significant fraction of the gaseous oxygen budget, leading to a gas-phase C/O of ~ 1 in the disk surface between the H_2O and CO midplane icelines.

4. H_2^{18}O Upper Limits

To see if our picture of a vertical water snowline holds, we looked at published and archival ALMA data of H_2O lines with lower upper level energies than the $10_{2,9}-9_{3,6}$ water line, which should better trace the 150–300 K water vapor. This encompasses two ($5_{1,5}-4_{2,2}$) H_2^{18}O nondetections (Carr et al. 2018; Notsu et al. 2019) toward AS 205 and HD 163296 as well as two previously unpublished 390.608 GHz, $4_{1,4}-3_{2,1}$ H_2^{18}O , $E_{\text{up}} = 322$ K, nondetections toward RNO 90 and HD 163296 (in 100 and 40 minutes with ALMA, respectively, 2015.1.00847.S, PI Du, F). Figure 3 shows the nondetection of the $4_{1,4}-3_{2,1}$ H_2^{18}O line in the product data toward both disks, together with the nondetection of the $5_{1,5}-4_{2,2}$ H_2^{18}O water line toward AS 205 (Carr et al. 2018). To put these line observations in context, Table 1 summarizes some source properties for these systems.

The nondetections toward T-Tauri stars AS 205 and RNO 90 are consistent with a small snowline radius (taken to be 1.8 au following the other results for AS 205) and a gas–dust temperature contrast of 450 K at the H_2O snowline, following the H_2O and ^{13}CO rovibrational temperature derived toward AS 205 at this radius (Salyk et al. 2011a, 2011b). We find a 3σ flux upper limit between -14 and 22 km s^{-1} of 84 mJy km s^{-1} for AS 205, and a 3σ flux upper limit between -17 and 19 km s^{-1} of 90 mJy km s^{-1} for RNO 90.

No mid-infrared water lines have been detected toward Herbig Ae star HD 163296, as is typical for these systems (Pontoppidan et al. 2010b). As such no mid-infrared derived snowline radius is available. Based on thermochemical modeling, Notsu et al. (2016) estimate a water snowline radius of 7 au. We make a simple prediction for the line flux for HD 163296, taking a low estimate for the gas temperature in the surface layer, 300 K at the 7 au snowline radius. This results in a model line flux of 380 mJy km s^{-1} , compared to the 500 mJy km s^{-1} prediction of a Herbig Ae disk (Notsu et al. 2018). This would have been detected at $>3\sigma$, which corresponds to 290 mJy km s^{-1} between -13 and 23 km s^{-1} . This is consistent with the nondetection of the water lines around 322 GHz (Notsu et al. 2019) and implies either a smaller emitting region, or optically thick dust at 300–400 GHz in the warm molecular layer suppressing water line emission.

5. Summary

We have re-examined the detection of the water line at 321.2256 GHz toward AS 205 N from Carr et al. (2018) and in light of water emission line constraints on the inner disk of AS 205 N conclude that this line is a maser originating from the water reservoir within the midplane snowline of the AS 205 N. Furthermore, we propose that vertical mixing and dust settling have a strong impact on the abundance of water above the surface snowline, creating a jump profile in the water abundance at the location of the midplane snowline, with a low H_2O abundance outside the water snowline. Warm water emission thus always traces the emitting area within the water midplane snowline. This explains the lack of H_2^{18}O water line

detections with ALMA to date as well as suggests we can use masing H_2^{16}O transitions such as the line at 321.2256 GHz to kinematically probe the water snowline location down to radii that ALMA would otherwise not be sensitive to.

This paper makes use of the following ALMA data: ADS/JAO.ALMA#2015.1.00847.S, ADS/JAO.ALMA#2016.1.00549.S. ALMA is a partnership of ESO (representing its member states), NSF (USA) and NINS (Japan), together with NRC (Canada), MOST and ASIAA (Taiwan), and KASI (Republic of Korea), in cooperation with the Republic of Chile. The Joint ALMA Observatory is operated by ESO, AUI/NRAO and NAOJ. The National Radio Astronomy Observatory is a facility of the National Science Foundation operated under cooperative agreement by Associated Universities, Inc. A.D.B. and E.A.B. acknowledge support from NSF Grant#1907653 and NASA grant XRP 80NSSC20K0259.

Software: Astropy (Astropy Collaboration et al. 2013, 2018), SciPy (Virtanen et al. 2020), NumPy (Van Der Walt et al. 2011), Matplotlib (Hunter 2007), RADEX (van der Tak et al. 2007).

ORCID iDs

Arthur D. Bosman  <https://orcid.org/0000-0003-4001-3589>

Edwin A. Bergin  <https://orcid.org/0000-0003-4179-6394>

References

- Andrews, S. M., Huang, J., Pérez, L. M., et al. 2018, *ApJL*, **869**, L41
- Astropy Collaboration, Price-Whelan, A. M., Sipőcz, B. M., et al. 2018, *AJ*, **156**, 123
- Astropy Collaboration, Robitaille, T. P., Tollerud, E. J., et al. 2013, *A&A*, **558**, A33
- Banzatti, A., Pontoppidan, K. M., Salyk, C., et al. 2017, *ApJ*, **834**, 152
- Bergin, E. A., Hogerheijde, M. R., Brinch, C., et al. 2010, *A&A*, **521**, L33
- Blevins, S. M., Pontoppidan, K. M., Banzatti, A., et al. 2016, *ApJ*, **818**, 22
- Bosman, A. D., Bruderer, S., & van Dishoeck, E. F. 2017, *A&A*, **601**, A36
- Bosman, A. D., Tielens, A. G. G. M., & van Dishoeck, E. F. 2018, *A&A*, **611**, A80
- Bruderer, S., Harsono, D., & van Dishoeck, E. F. 2015, *A&A*, **575**, A94
- Carr, J. S., & Najita, J. R. 2008, *Sci*, **319**, 1504
- Carr, J. S., & Najita, J. R. 2011, *ApJ*, **733**, 102
- Carr, J. S., Najita, J. R., & Salyk, C. 2018, *RNAAS*, **2**, 169
- Ciesla, F. J., & Cuzzi, J. N. 2006, *Icar*, **181**, 178
- Cockell, C. S., Bush, T., Bryce, C., et al. 2016, *AsBio*, **16**, 89
- Daniel, F., Dubernet, M. L., & Grosjean, A. 2011, *A&A*, **536**, A76
- Du, F., Bergin, E. A., Hogerheijde, M., et al. 2017, *ApJ*, **842**, 98
- Gray, M. D., Baudry, A., Richards, A. M. S., et al. 2016, *MNRAS*, **456**, 374
- Harsono, D., Bruderer, S., & van Dishoeck, E. F. 2015, *A&A*, **582**, A41
- Harsono, D., Persson, M. V., Ramos, A., et al. 2020, *A&A*, **636**, A26
- Hayashi, C. 1981, *PTthPS*, **70**, 35
- Hogerheijde, M. R., Bergin, E. A., Brinch, C., et al. 2011, *Sci*, **334**, 338
- Hunter, J. D. 2007, *CSE*, **9**, 90
- Ida, S., Yamamura, T., & Okuzumi, S. 2019, *A&A*, **624**, A28
- Kama, M., Bruderer, S., van Dishoeck, E. F., et al. 2016, *A&A*, **592**, A83
- Krijt, S., Bosman, A. D., Zhang, K., et al. 2020, *ApJ*, **899**, 134
- Krijt, S., Ciesla, F. J., & Bergin, E. A. 2016, *ApJ*, **833**, 285
- Krijt, S., Schwarz, K. R., Bergin, E. A., & Ciesla, F. J. 2018, *ApJ*, **864**, 78
- Kruijer, T. S., Kleine, T., & Borg, L. E. 2020, *NatAs*, **4**, 32
- Lingam, M., & Loeb, A. 2019, *AJ*, **157**, 25
- Madhusudhan, N. 2019, *ARA&A*, **57**, 617
- Meijerink, R., Pontoppidan, K. M., Blake, G. A., Poelman, D. R., & Dullemond, C. P. 2009, *ApJ*, **704**, 1471
- Morbidelli, A., Bitsch, B., Crida, A., et al. 2016, *Icar*, **267**, 368
- Morbidelli, A., Chambers, J., Lunine, J. I., et al. 2000, *M&PS*, **35**, 1309
- Mulders, G. D., Ciesla, F. J., Min, M., & Pascucci, I. 2015, *ApJ*, **807**, 9
- Najita, J. R., Carr, J. S., Salyk, C., et al. 2018, *ApJ*, **862**, 122
- Neufeld, D. A., & Melnick, G. J. 1991, *ApJ*, **368**, 215
- Notsu, S., Akiyama, E., Booth, A., et al. 2019, *ApJ*, **875**, 96
- Notsu, S., Nomura, H., Ishimoto, D., et al. 2016, *ApJ*, **827**, 113
- Notsu, S., Nomura, H., Walsh, C., et al. 2018, *ApJ*, **855**, 62
- Patel, N. A., Curiel, S., Zhang, Q., et al. 2007, *ApJL*, **658**, L55
- Pontoppidan, K. M., Blake, G. A., & Smette, A. 2011, *ApJ*, **733**, 84
- Pontoppidan, K. M., & Blevins, S. M. 2014, *FaDi*, **169**, 49
- Pontoppidan, K. M., Salyk, C., Bergin, E. A., et al. 2014, in *Protostars and Planets VI*, ed. H. Beuther et al. (Tucson, AZ: Univ. Arizona Press), 363
- Pontoppidan, K. M., Salyk, C., Blake, G. A., & Käuffel, H. U. 2010a, *ApJL*, **722**, L173
- Pontoppidan, K. M., Salyk, C., Blake, G. A., et al. 2010b, *ApJ*, **720**, 887
- Salyk, C., Blake, G. A., Boogert, A. C. A., & Brown, J. M. 2011a, *ApJ*, **743**, 112
- Salyk, C., Lacy, J., Richter, M., et al. 2019, *ApJ*, **874**, 24
- Salyk, C., Pontoppidan, K. M., Blake, G. A., Najita, J. R., & Carr, J. S. 2011b, *ApJ*, **731**, 130
- van der Tak, F. F. S., Black, J. H., Schöier, F. L., Jansen, D. J., & van Dishoeck, E. F. 2007, *A&A*, **468**, 627
- Van Der Walt, S., Colbert, S. C., & Varoquaux, G. 2011, *CSE*, **13**, 22
- van Dishoeck, E. F., Kristensen, L. E., Mottram, J. C., et al. 2021, *A&A*, **648**, A24
- Virtanen, P., Gommers, R., Oliphant, T. E., et al. 2020, *NatMe*, **17**, 261
- Woitke, P., Kamp, I., Antonellini, S., et al. 2019, *PASP*, **131**, 064301
- Zhang, K., Bergin, E. A., Schwarz, K., Krijt, S., & Ciesla, F. 2019, *ApJ*, **883**, 98